J. Fluid Mech. (2000), *vol.* 418, *pp.* 297–312. Printed in the United Kingdom

Three-dimensional instabilities of steady double-diffusive interleaving

By OLIVER S. KERR

Department of Mathematics, City University,
Northampton Square, London EC1V 0HB, UK

(Received 10 February 2000)

A stratified body of fluid with compensating horizontal temperature and salinity gradients can undergo an interleaving instability which takes the form of almost horizontal intrusions. As the amplitude of these intrusions grows they can undergo secondary instabilities which eventually leads to the mixing of the fluid in the interior of the intrusions. A previous study of the secondary instabilities focused on two-dimensional disturbances. These corresponded to experimental observations of that time which all seemed to indicate that flows were indeed two-dimensional. Some more recent experiments have shown that the initial secondary instability can make the flow three-dimensional, with the secondary instabilities taking the form of rolls with their axes aligned with the direction of the flow in the intrusions. Here we present a three dimensional stability analysis of steady finite-amplitude intrusions and look at the circumstances which can lead to the three-dimensional instabilities being more likely to be observed.

1. Introduction

The presence of horizontal temperature and salinity gradients in a stratified fluid can lead to the development of instabilities that take the form of almost horizontal intrusions. These were initially investigated by Stern (1967) who assumed that the fluxes of heat and salt were dominated by the presence of salt fingers (Stern 1960). However this almost horizontal layering can also develop when the fluxes are driven purely by molecular diffusivities and can occur in stratified fluid in containers (Thorpe, Hutt & Soulsby 1969; Chen, Briggs & Wirtz 1971; and others) as well as unbounded fluids (Holyer 1983). Holyer noted that as the intrusions grow the vertical temperature and salinity gradients in their interior become conducive to secondary instabilities. Indeed the development of instabilities inside the intrusion have been observed in numerous experiments (for example Tsinober, Yahalom & Shlien 1983; Tanny & Tsinober 1988) and numerical simulations (for example Schladow, Thomas & Koseff 1992; Dijkstra & Kranenborg 1998; Kranenborg & Dijkstra 1998). Nearly all the experiments view the intrusions from the side (i.e. viewed horizontally and perpendicularly to the horizontal temperature and salinity gradients). The observed secondary instabilities often seem to be purely two-dimensional. In addition, all the numerical investigations to date that reveal these secondary instabilities to intrusions have also been two-dimensional. For this reason the original investigation of Kerr (1992) into instabilities of double-diffusive intrusions focused on such two-dimensional instabilities. However, more recently experiments by Chen & Chen (1997) have clearly shown that secondary instabilities can appear inside a convecting layer that consist

of rolls whose axes are perpendicular to those of the primary instabilities. In their experiments they viewed the convecting fluid from above, clearly revealing the three-dimensionality of the flow in some experiments. This three-dimensional nature of the flow is also shown in the exploratory experiments of Biello (1997) where a narrow slot containing a salt-stratified fluid was heated from one wall. The opposite wall was transparent and exposed to the ambient air temperature. Horizontal layered convection occurred in which secondary instabilities in the plane of the walls were clearly visible. The purpose of the investigation presented here is to extend the previous analysis to allow for arbitrary orientation of the disturbances to the intrusions and so give an insight into when these instabilities to intrusions are likely to be two-dimensional, and when they are likely to be three-dimensional.

The analysis of the stability of intrusions which are growing exponentially with time poses mathematical difficulties, and so we follow Holyer (1981), in her analysis of the stability of salt fingers, and Kerr (1992) by examining the stability of intrusions parallel to the fastest growing modes, but with a thickness chosen so that they have zero growth rate. In § 2 we will derive the governing equations for the secondary instabilities to these steady intrusions. The solutions of these linear stability equations will be investigated in § 3, where we will restrict ourselves to examining situations where there is no mean vertical temperature gradient and the horizontal salinity gradient is no bigger than the vertical gradient. It will be found that under the assumptions made here the preferred instabilities can be both two-dimensional and three-dimensional. In § 4 we will examine the asymptotics for relatively weak horizontal gradients for instabilities whose axes are aligned in the direction of the horizontal gradients. This analysis essentially quantifies the arguments of Holyer (1983) and of Chen & Chen (1997) who anticipated that instabilities should appear when the vertical gradients locally are favourable to salt fingering. It also provides a predicted length scale for the disturbances. The implications of this work for real intrusions are discussed in the concluding remarks in § 5.

2. Governing equations

We consider the stability of intrusions in an unbounded fluid with constant vertical and horizontal salinity and temperature gradients. We only consider the case where there is no nett horizontal density gradient. Holyer (1983) showed that such a fluid was always unstable to linear perturbations and observed that a single mode could grow to arbitrary amplitude and still satisfy the full nonlinear equations. The analysis of, say, the stability of the fastest growing mode of instability poses mathematical difficulties. We use the same approach as Kerr and look at the stability of steady-state intrusions whose wavevector is parallel to that of the fastest growing mode.

The velocity, temperature and salinity are given by

$$\boldsymbol{u}(x,y,z,t) = \hat{\boldsymbol{U}}(x,z) + \boldsymbol{u}'(x,y,z,t), \tag{2.1}$$

$$T(x,y,z,t) = T_0 + x\overline{T}_x + z\overline{T}_z + \hat{T}(x,z) + T'(x,y,z,t), \tag{2.2}$$

$$S(x,y,z,t) = S_0 + x\overline{S}_x + z\overline{S}_z + \hat{S}(x,z) + S'(x,y,z,t), \tag{2.3}$$

where the background temperature and salinity gradients, $\overline{T}_x$, $\overline{T}_z$, $\overline{S}_x$ and $\overline{S}_z$ are all constant. The interleaving is given by $\hat{\boldsymbol{U}}$, $\hat{T}$ and $\hat{S}$ while the perturbations to these are given by $\boldsymbol{u}'$, T' and S'. The density of the fluid is given by

$$\rho = \rho_0(1 - \alpha(T - T_0) + \beta(S - S_0)), \tag{2.4}$$

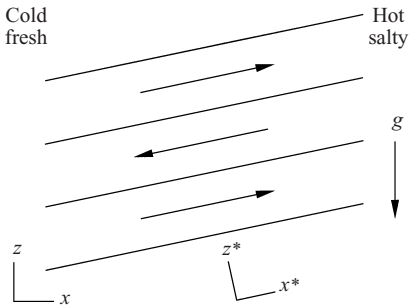

FIGURE 1. Schematic diagram showing the geometry under consideration.

where α is the coefficient of thermal expansion and β the coefficient of density increase with respect to the addition of salt. The requirement that there is no horizontal density gradient implies that

$$\alpha \overline{T}_x = \beta \overline{S}_x. \tag{2.5}$$

We assume that these are both positive.

The linearized equations for the perturbations to the interleaving layers are

$$\frac{\partial \boldsymbol{u}'}{\partial t} + \hat{\boldsymbol{U}} \cdot \nabla \boldsymbol{u}' + \boldsymbol{u}' \cdot \nabla \hat{\boldsymbol{U}} = -\frac{1}{\rho} \nabla p' + g(\alpha T' - \beta S')\hat{\boldsymbol{z}} + \nu \nabla^2 \boldsymbol{u}', \tag{2.6}$$

$$\frac{\partial T'}{\partial t} + \hat{\boldsymbol{U}} \cdot \nabla T' + \boldsymbol{u}' \cdot \nabla \hat{T} + u\overline{T}_x + w\overline{T}_z = \kappa_T \nabla^2 T', \tag{2.7}$$

$$\frac{\partial S'}{\partial t} + \hat{\boldsymbol{U}} \cdot \nabla S' + \boldsymbol{u}' \cdot \nabla \hat{S} + u\overline{S}_x + w\overline{S}_z = \kappa_S \nabla^2 S'. \tag{2.8}$$

Here g is the acceleration due to gravity, ν the kinematic viscosity, κ_T the diffusivity of heat, κ_S the diffusivity of salt and $\hat{\boldsymbol{z}}$ the unit vector pointing in the vertical direction.

We follow Holyer (1981) and Kerr (1992) and use the inverse of the wavenumber of the fastest growing interleaving mode, $|\mu|^{-1}$, as a length scale for the non-dimensionalization of these equations, $(\mu^2 \kappa_T)^{-1}$ for time, $\nu\kappa_T|\mu|^3/(g\alpha)$ for temperature and $\nu\kappa_T|\mu|^3/(g\beta)$ for the salinity. The magnitudes of the temperature and salinity gradients are measured by three Rayleigh numbers: the horizontal Rayleigh number H and the vertical temperature and salt Rayleigh numbers R_T and R_S. These are defined by

$$H = \frac{g\beta\overline{S}_x}{\nu\kappa_T\mu^4}, \quad R_T = \frac{g\beta\overline{T}_z}{\nu\kappa_T\mu^4}, \quad R_S = \frac{g\beta\overline{S}_z}{\nu\kappa_T\mu^4}. \tag{2.9}$$

These Rayleigh numbers are not mutually independent. They are determined by the *ratios* of the vertical and horizontal gradients, along with the slope of the intrusions and their non-dimensional growth rate. The physical scale of the fastest growing intrusions can then be determined from the above equations. For further details of these scalings see Holyer (1983).

We will diverge slightly from Kerr (1992) by aligning our axes with the interleaving layers (see figure 1), and so the wavevector for the fastest growing mode will only have one non-zero component parallel to the z^*-axis. This is done to ease finding and describing the fastest growing modes of instability. Just as for the two-dimensional case these are often only weakly dependent on the component of the wavevector perpendicular to the plane of the intrusions.

All subsequent equations are non-dimensional. The marginally stable interleaving mode whose wavenumber is parallel to that of the fastest growing mode has velocity, temperature and salinity given by

$$\hat{\boldsymbol{U}} = (\hat{U}^*, 0, 0)\cos \hat{m}^* z^*, \qquad \hat{T} = \hat{T}^* \cos \hat{m}^* z^*, \qquad \hat{S} = \hat{S}^* \cos \hat{m}^* z^*, \tag{2.10}$$

where $\hat{m}^*$, $\hat{U}^*$, $\hat{T}^*$ and $\hat{S}^*$ satisfy

$$0 = \sin\theta(\hat{T}^* - \hat{S}^*) - \hat{m}^{*2}\hat{U}^*, \tag{2.11}$$

$$(H\cos\theta + R_T \sin\theta)\hat{U}^* = -\hat{m}^{*2}\hat{T}^*, \tag{2.12}$$

$$(H\cos\theta + R_S \sin\theta)\hat{U}^* = -\tau\hat{m}^{*2}\hat{S}^*, \tag{2.13}$$

where θ is the angle between the interleaving layers and the horizontal, again see Holyer (1983) for details. For non-trivial solutions to exist $\hat{m}^*$ must satisfy

$$\hat{m}^{*4} = \frac{1-\tau}{2\tau} H \sin 2\theta + \frac{R_S - \tau R_T}{\tau} \sin^2\theta. \tag{2.14}$$

Since θ is determined by the fastest growing intrusions, it is clear from this that the size of the zero-growth-rate intrusions parallel to the fastest growing intrusions is uniquely defined.

The non-dimensional equations for the perturbations, after dropping the asterisks, are

$$\frac{1}{\sigma}\left[\frac{\partial u'}{\partial t} + \hat{U}\cos\hat{m}z\frac{\partial u'}{\partial x} - \hat{m}w'\hat{U}\sin\hat{m}z\right] = -\frac{\partial p'}{\partial x} + \sin\theta(T' - S') + \nabla^2 u', \tag{2.15}$$

$$\frac{1}{\sigma}\left[\frac{\partial v'}{\partial t} + \hat{U}\cos\hat{m}z\frac{\partial v'}{\partial x}\right] = -\frac{\partial p'}{\partial y} + \nabla^2 v', \tag{2.16}$$

$$\frac{1}{\sigma}\left[\frac{\partial w'}{\partial t} + \hat{U}\cos\hat{m}z\frac{\partial w'}{\partial x}\right] = -\frac{\partial p'}{\partial z} + \cos\theta(T' - S') + \nabla^2 w', \tag{2.17}$$

$$\frac{\partial u'}{\partial x} + \frac{\partial v'}{\partial y} + \frac{\partial w'}{\partial z} = 0, \tag{2.18}$$

$$\frac{\partial T'}{\partial t} + \hat{U}\cos\hat{m}z\frac{\partial T'}{\partial x} - \hat{m}w'\hat{T}\sin\hat{m}z + u'(H\cos\theta + R_T\sin\theta) + w'(R_T\cos\theta - H\sin\theta) = \nabla^2 T', \tag{2.19}$$

$$\frac{\partial S'}{\partial t} + \hat{U}\cos\hat{m}z\frac{\partial S'}{\partial x} - \hat{m}w'\hat{S}\sin\hat{m}z + u'(H\cos\theta + R_S\sin\theta) + w'(R_S\cos\theta - H\sin\theta) = \tau\nabla^2 S'. \tag{2.20}$$

The solutions to these can be expressed in Floquet form:

$$(u', v', w', p', T', S') = \exp\left[\lambda t + \mathrm{i}(kx + ly + mz)\right] \sum_{n=-\infty}^{\infty} (u_n, v_n, w_n, -\mathrm{i}p_n, T_n, S_n)\exp(\mathrm{i}n\hat{m}z). \tag{2.21}$$

Note the inclusion of a factor of $-\mathrm{i}$ before the p_n to ensure the equations now have

real coefficients. This expansion gives rise to the set of equations for each n:

$$\frac{1}{\sigma}\left[\lambda u_n - \frac{k\hat{U}}{2}(u_{n+1} - u_{n-1}) + \frac{\hat{m}\hat{U}}{2}(w_{n+1} + w_{n-1})\right]$$
$$= -kp_n + \sin\theta(T_n - S_n) + (k^2 + l^2 + (m + n\hat{m})^2)u_n, \quad (2.22)$$

$$\frac{1}{\sigma}\left[\lambda v_n - \frac{k\hat{U}}{2}(v_{n+1} - v_{n-1})\right] = -lp_n + (k^2 + l^2 + (m + n\hat{m})^2)v_n, \quad (2.23)$$

$$\frac{1}{\sigma}\left[\lambda w_n - \frac{k\hat{U}}{2}(w_{n+1} - w_{n-1})\right]$$
$$= -(m + n\hat{m})p_n + \cos\theta(T_n - S_n) - \sigma(k^2 + l^2 + (m + n\hat{m})^2)w_n, \quad (2.24)$$

$$0 = ku_n + lv_n + (m + n\hat{m})w_n, \quad (2.25)$$

$$\lambda T_n + (H\cos\theta + R_T\sin\theta)u_n + (-H\sin\theta + R_T\cos\theta)w_n$$
$$-\frac{k\hat{U}}{2}(T_{n+1} - T_{n-1}) + \frac{\hat{m}\hat{T}}{2}(w_{n+1} + w_{n-1}) = -(k^2 + l^2 + (m + n\hat{m})^2)T_n, \quad (2.26)$$

$$\lambda S_n + (H\cos\theta + R_T\sin\theta)u_n + (-H\sin\theta + R_T\cos\theta)w_n$$
$$-\frac{k\hat{U}}{2}(S_{n+1} - S_{n-1}) + \frac{\hat{m}\hat{S}}{2}(w_{n+1} + w_{n-1}) = -\tau(k^2 + l^2 + (m + n\hat{m})^2)S_n. \quad (2.27)$$

These can be expressed in terms of infinite matrices

$$\boldsymbol{A}\boldsymbol{x} = \lambda\boldsymbol{B}\boldsymbol{x}, \quad (2.28)$$

where $\boldsymbol{x}$ is a column vector which is the transpose of $(\ldots, u_n, v_n, w_n, p_n, T_n, S_n, \ldots)$ and $\boldsymbol{B}$ is a diagonal matrix with either 1 or 0 in its diagonal entries. The eigenvalues and corresponding eigenvectors of a truncated form of this matrix can be calculated. The level of truncation of the matrix system was chosen to ensure an appropriate degree of accuracy. Typically the truncation level was chosen so that the eigenvectors contained 6×25 terms, although more terms were used for accuracy checking and when the disturbances became smaller. Here routines from the NAG numerical library were used. In each case the mode whose eigenvalue has the largest real part was identified as the most unstable mode.

3. Results

In this section we will assume that the fluid has Prantl number $\sigma = 10$ and salt/heat diffusivity ratio $\tau = 1/100$. These are the values used in Kerr (1992) and are used here for compatibility. Calculations have also been done with $\sigma = 7$ and $\tau = 1/80$ which would be more appropriate in a laboratory. The results of these two sets of calculations show little qualitative difference. We shall also restrict ourselves to the case $R_T = 0$ with $R_S < 0$ in this section since this corresponds to nearly all laboratory experiments and numerical simulations where layered convection has been observed.

Since the marginally stable interleaving mode chosen as the background state is

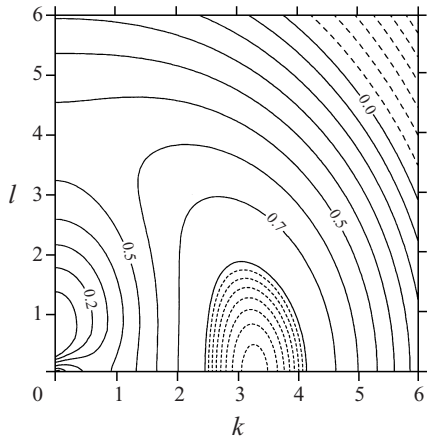

FIGURE 2. Contour plots of the fastest growth rate as functions of k and l for $|H/R_S| = 1/5$. The solid contours start from 0 with spacing 0.1, the long-dashed lines are for negative growth rate with spacing 0.1, and the short-dashed contours near the peak have spacing 0.01.

parallel to the fastest growing interleaving mode they do not interact via the nonlinear terms. This means that the fastest growing mode is still a mode of instability which will appear from the stability analysis. For any other mode to be observed it would have to have a growth rate at least as fast as this one. Thus we shall follow Kerr (1992) and look for parameter regimes where the fastest growing mode of instability has a growth rate as least as big as that of the fastest growing interleaving mode, and define marginal stability to be the case where the growth rates are the same.

The first example we will look at has $|H/R_S| = 1/5$ and $R_T = 0$. The absence of a vertical temperature gradient and the vertical salinity gradient being stronger than the horizontal gradient is typical of experiments. When the fastest growing mode distinct from the interleaving mode is found by optimizing k, l and m it is determined that the growth rate does not depend strongly on m. This is an indication that the instabilities are essentially localized in the core of the intrusions with only weak linking between adjacent layers. For the sake of simplicity we will concentrate on presenting the results of varying k and l. In all cases the solutions have also been optimized by varying m even if not explicitly stated.

The growth rate for secondary instabilities as a function of k and l is shown in figure 2 for the case where the amplitude of the interleaving is such that there first appears a marginally stable mode distinct from the interleaving mode. Due to the symmetry of the problem we can restrict ourselves to the case where both k and l are non-negative. The plots for other quadrants can be found by reflecting these contours in the axes. There is a sharp peak at the origin which corresponds to the fastest growing interleaving mode. As we are using axes aligned with this fastest growing intrusion this mode has $k = l = 0$. Surrounding this peak is an approximately elliptical ring where there is strong growth. This has a maximum on the k-axis at $k = 3.268$ and a saddle point on the l-axis at $l = 3.775$. Thus the fastest growing instabilities in this case are just the two-dimensional instabilities investigated previously in Kerr (1992).

The amplitude of the background intrusions used for figure 2 that gives rise to the two-dimensional instabilities with the same growth rate as the interleaving mode is $\hat{U} = \hat{\psi}\hat{m} = 0.09558\,\hat{m}$. Here $\hat{\psi}$ is the amplitude of the stream function that was used

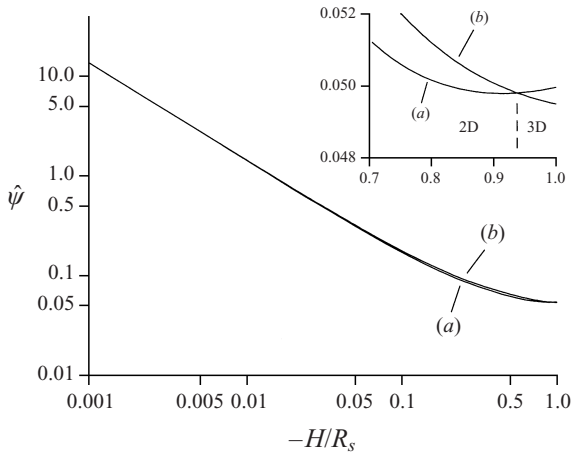

FIGURE 3. Graph of the magnitude of the interleaving $\hat{\psi}$ corresponding to marginal instability for (*a*) the two-dimensional mode, $l = 0$ and (*b*) the three-dimensional mode, $k = 0$. The inset shows an enlargement of the region where the two lines cross, with the regions where two- and three-dimensional instabilities are most unstable indicated.

to describe the amplitude of the intrusions in Kerr (1992). For the sake of consistency we will also use $\hat{\psi}$ here as a measure of the amplitude of these steady intrusions. If the amplitude of the intrusions is increased to $\hat{\psi} = 0.10008$ then the growth rates all the way around the almost elliptical ridge around the central peak exceed that of the interleaving mode. This is only a small increase in the amplitude compared to the two-dimensional $l = 0$ mode. The relative closeness of the point of onset of the different modes of instability may have consequences for which instabilities are observed in real situations where there may be geometrical constraints on the possible modes of instabilities which would favour the three-dimensional modes. This will be discussed later.

The results for $|H/R_S| = 1/5$ are qualitatively similar to those for nearly all values of the ratio $|H/R_S|$. In figure 3 the amplitude of the background intrusions which support modes with growth rate equal to the fastest growing interleaving mode are shown for a large range of the ratio $|H/R_S|$. There are two lines plotted, one corresponding to modes with $l = 0$ and one to modes with $k = 0$. These are very close for all points on the graphs, and are often hard to distinguish. For nearly all values of $|H/R_S|$ the two-dimensional mode with $l = 0$ occurs first and is the fastest growing mode of instability. However, when $|H/R_S| = 0.9381$ the two lines cross over. This section is enlarged in the inset in the figure. The contour plots for the growth rates at this transition point as functions of k and l are shown in figure 4. Here it can be seen that the peak of the growth rate surface is almost circular with no discernible single maximum at this resolution. The abrupt change in the contour spacing in the top right corner of figure 4 is due to a change in the mode with fastest growth rate to one which is less sensitive to changes in k and l.

One feature of the three-dimensional modes which differs from the two-dimensional modes is the size of the instabilities. The variation in the horizontal wavenumber, l, for the three-dimensional marginally stable modes is shown by the solid line in figure 5. This shows a steady rise in l as $|H/R_S|$ decreases. This rise continues beyond the values shown here, but a combination of the decreasing size of the instabilities which requires a much larger truncation in the matrix equation, and the rapidly

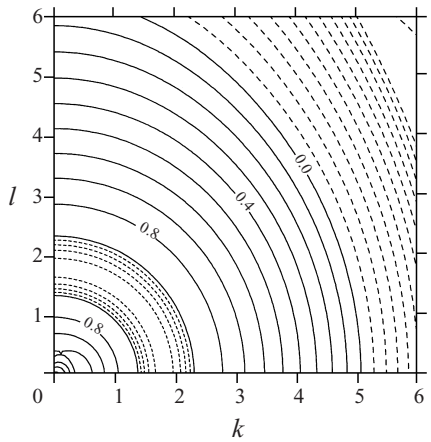

FIGURE 4. Contour plots of the fastest growth rate as functions of k and l for $|H/R_S| = 0.9381$. The solid contours start from 0 with spacing 0.1, the long-dashed lines are for negative growth rate with spacing 0.1, and the short-dashed contours near the peak have spacing 0.01.

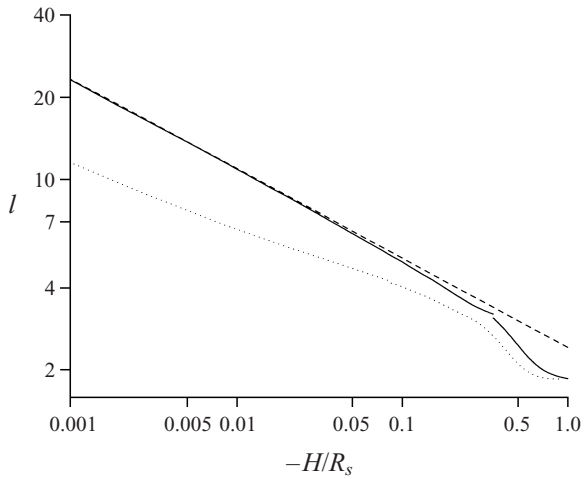

FIGURE 5. Graph of the horizontal wavenumber l for the marginally stable three-dimensional mode, $k = 0$, as a function of the gradient ratio $|H/R_S|$ (solid line). Superimposed is the asymptotic prediction from § 4 (dashed line), and k as a function of $|H/R_S|$ from Kerr (1992) (dotted line).

increasing sensitivity of the fastest growth rate and the corresponding wavenumbers to variations in the value of $\hat{\psi}$, lead to a deterioration in the numerical accuracy. Superimposed on this graph is the asymptotic prediction from the next section which is a straight line of slope $-1/3$ (the dashed line). The horizontal component of the wavenumber in the two-dimensional case, shown by the dotted line, increases more slowly as $|H/R_S|$ decreases. For lower values of $|H/R_S|$ than shown there is a transition after which it subsequently declines (Kerr 1992), indicating that the horizontal extent of the instabilities increases, in contrast to the three-dimensional case where they get ever smaller.

The graph of the wavenumber of the marginal modes with $k = 0$ has one other visible feature of note. Towards the right-hand end there is a small jump in the optimum wavenumber. This is not the only point where there is a jump, but the only

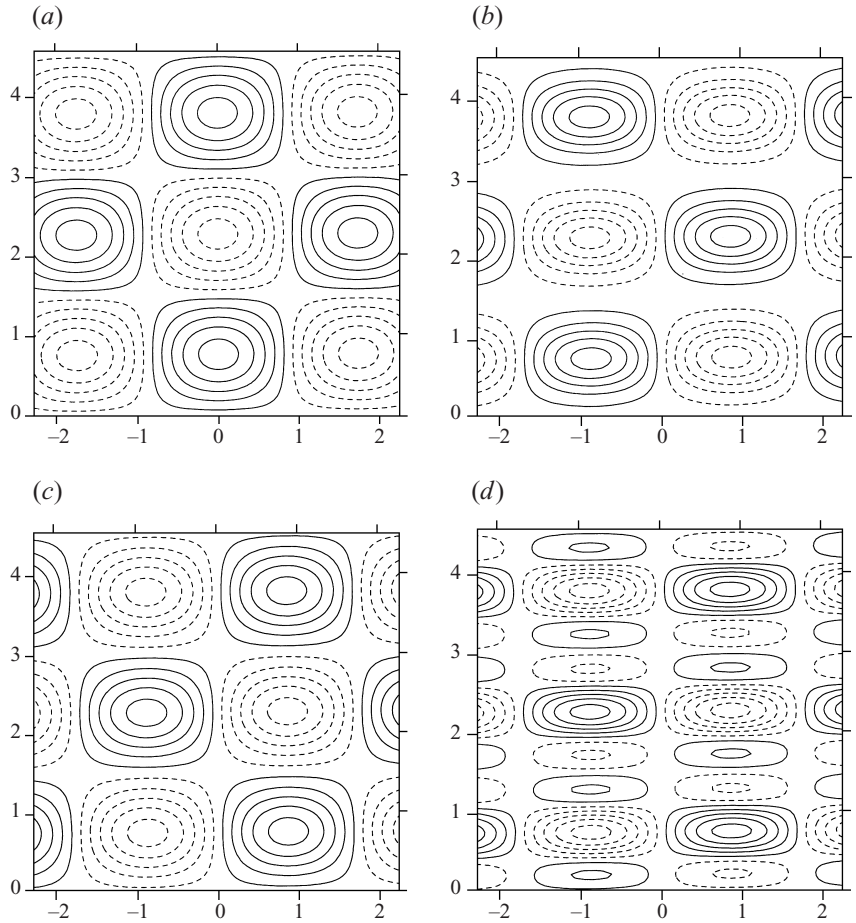

FIGURE 6. Plots of the marginally stable perturbations in the (y, z)-plane for $|H/R_S| = 1$, showing (*a*) streamlines, (*b*) u', (*c*) T' and (*d*) S'. The solid lines show contours for 10%, 30%, 50%, 70% and 90% of the maximum values and the dashed lines show the corresponding negative contours.

one visible at the resolution of this graph. The reason behind this small jump can be appreciated from the plots of the three-dimensional instabilities shown in figures 6–8 for $|H/R_S| = 1$, $1/5$ and $1/20$ respectively. These show the streamlines of the instability in the (y, z)-plane, along with u', T' and S'. The disturbances are all located along the planes where the vertical density gradient is most reduced. Three of these regions are shown in figure 6 and two in each of figures 7 and 8. One clear difference between the cases with $|H/R_S| = 1$ and $1/20$ and the one with $|H/R_S| = 1/5$ is that in the latter case if the perturbations are shifted vertically by the height of an intrusion the picture is unaltered, while in the other cases the signs of the perturbations would be reversed. Which of the cases holds changes several times as $|H/R_S|$ decreases. As has already been mentioned, the growth rate of these instabilities is only weakly dependent on the third component of the wavenumber, m. Changing m changes the relative phases of adjacent rows of instabilities. The instabilities are essentially local and are little influenced by those in other rows. When there is a transition between the two possible cases the basic instabilities are little affected, hence the very small jump in the optimum l. As $|H/R_S|$ decreases the instabilities communicate even less

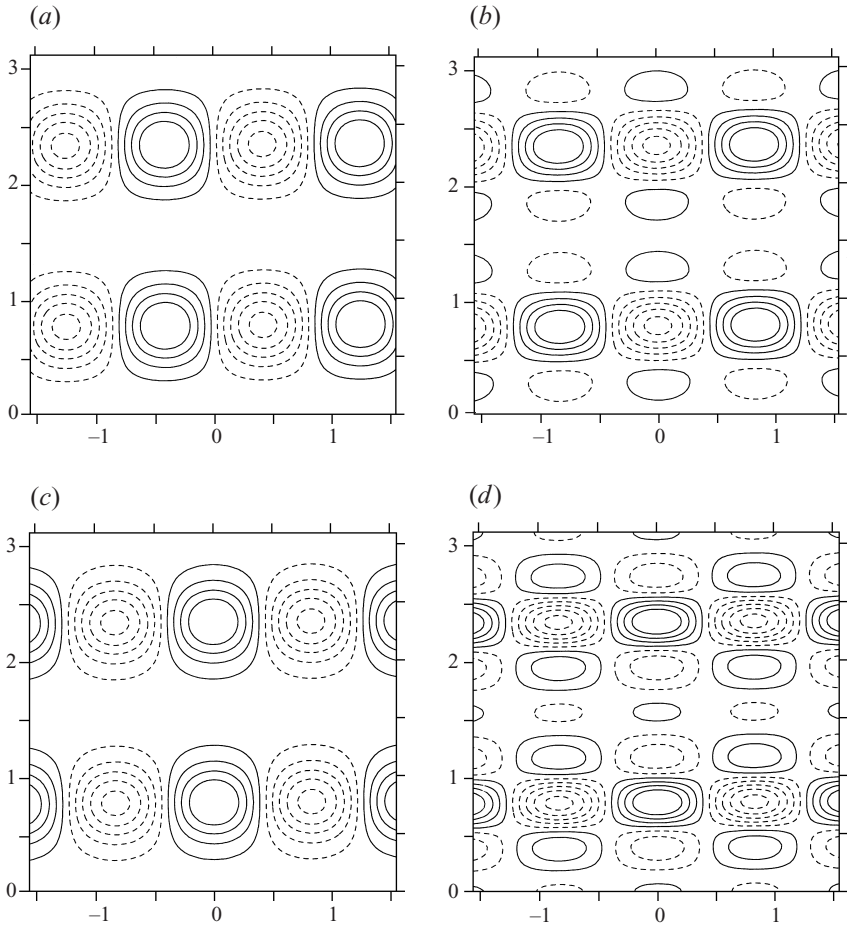

FIGURE 7. As figure 6 but for $|H/R_S| = 1/5$.

between rows, and so when there is a second transition between $|H/R_S| = 1/5$ and $1/20$ the effect is even smaller and the jump is not visible.

The sense of the circulation in the streamline plots in figures 6–8 is clockwise around the positive maxima. All these plots show features that would be expected from a salt-fingering instability growing in the region of the intrusions where the vertical density gradient is most reduced. When intrusions are driven by molecular diffusivities they have the general slope indicated in figure 1. Fluid in intrusions moving from left to right tends to be colder and fresher than the surrounding fluid, while fluid moving from right to left tends to be hotter and saltier. For salt fingering to occur the intrusions must grow sufficiently for hot salty water to lie over cooler fresher water. This will occur in the layers where there is a leftwards flow above and a rightwards flow below. Hence in a region of downflow in these three-dimensional instabilities there will be a local increase in the salinity and temperature, and because the fluid is moving from a leftward travelling region into a rightward travelling region its velocity perturbation u' will be negative. Conversely, if the flow is upwards then the temperature and salinity perturbations will be negative and the velocity perturbation will be positive. These features are shown in figures 6–8 where regions in the streamline plots (*a*) with a positive peak to the left and a negative peak to

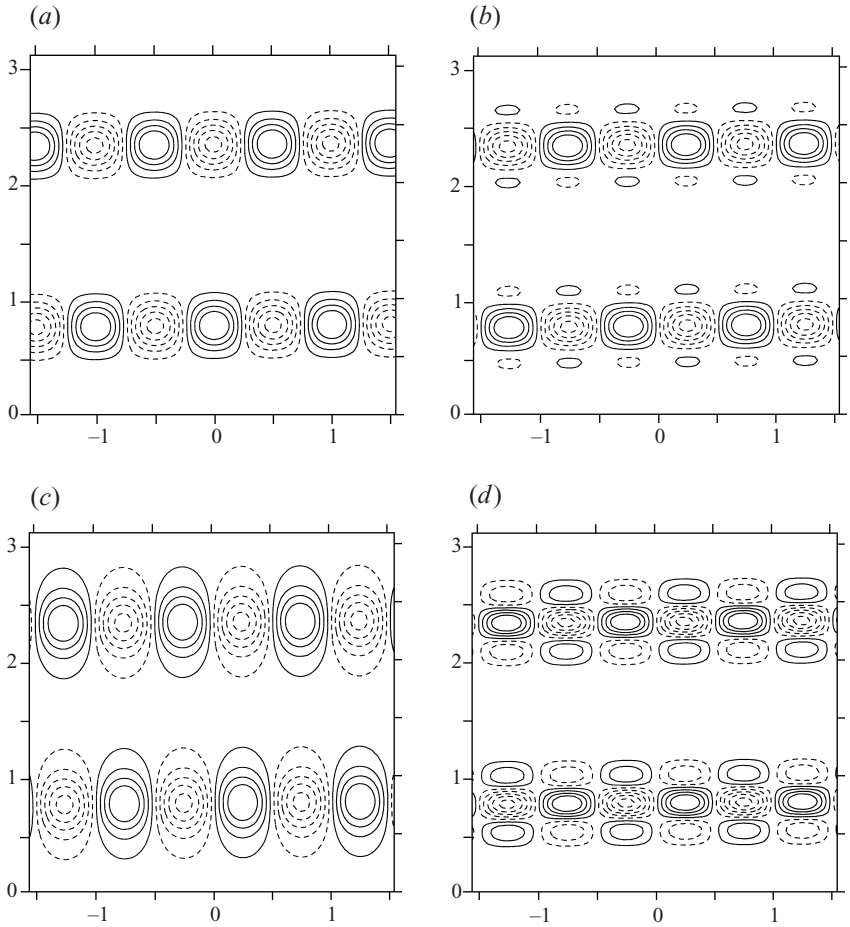

FIGURE 8. As figure 6 but for $|H/R_S| = 1/20$.

the right which correspond to upflows all show positive peaks in (*b*) u', and negative peaks in (*c*) T' and (*d*) S'.

Batchelor & Nitsche (1991) looked at convection in an unbounded fluid with the density varying sinusoidally in the vertical direction. A novel feature of their results is that a long-wavelength instability was found, with the denser layers of fluid sliding towards regions where the fluid had moved down and the lighter layers sliding towards the regions where the fluid had risen. The absence of a mean vertical density gradient results in there being no restoring force on regions of fluid which are displaced vertically. When such a gradient was present in their analysis, these modes of instability were not found. In the problem analysed here there is always a stable mean vertical density gradient superimposed on the vertical sinusoidal variations, and no equivalent long-wavelength modes of instability were found.

4. Asymptotics for weak horizontal gradients

The asymptotic analysis of the two-dimensional instabilities in the limit of weak horizontal gradients (i.e. when H is small compared to the the larger of $|R_T|$ and $|R_S|$) is given in Kerr (1992). There it was found that instabilities developed along the

line of maximum shear and maximum change to the vertical temperature and salinity gradients. It was clear from the local Richardson numbers that these instabilities were not shear driven, but were essentially localized double-diffusive intrusions. Although the previous results have indicated that in the limit of weak horizontal gradients this two-dimensional mode of instability dominates, we will look here at the three-dimensional modes of instability ($k = 0$) in this same limit. This will enable us to determine the relative importance of these two modes. It will also enable us to quantify the arguments of Holyer (1983) and Chen & Chen (1997) concerning the possible onset of localized double-diffusive convection in the core of the intrusions due to the change in the vertical temperature and salinity gradients, giving, for example, predictions for the wavelength of the instabilities.

When the horizontal gradients become relatively weak both the vertical and horizontal Rayleigh numbers become large as the physical size of the fastest growing modes, which is used in defining the Rayleigh numbers, tends to increase. However the vertical Rayleigh numbers increase at a faster rate than H. We follow Kerr and use $\epsilon = H^{-1}$ as an expansion parameter. As ϵ decreases both R_T and R_S (if non-zero) grow as ϵ^{-2} so the ratio of the horizontal gradients to the vertical gradients decreases as ϵ. The angle the intrusions make with the horizontal, θ, is at leading order proportional to ϵ, while the vertical wavenumber, $\hat{m}$ remains $O(1)$.

We shall find that the conjectures of Holyer (1983) and Chen & Chen (1997) that instabilities first appear when there is a region where the local vertical salinity and temperature gradients satisfy the condition for salt fingers is, to a first approximation, correct. This requires an $O(1)$ change to the background vertical gradients which will require the leading-order scalings $\hat{U} = O(\epsilon^{-1})$, $\hat{T} = O(\epsilon^{-2})$ and $\hat{S} = O(\epsilon^{-2})$. The most important difference between the two-dimensional case and the three-dimensional case under consideration here is that the dimension of the marginal instabilities tends to zero as $\epsilon \to 0$, unlike the two-dimensional case where the vertical scale remained $O(1)$ while the horizontal scale increased as ϵ^{-1}. For the moment we shall just say that the horizontal and vertical scales are proportional to ϵ^a and ϵ^b respectively, with both a and b positive, and that they are again localized along the regions of maximum change in the vertical temperature and salinity gradients.

We define rescaled quantities

$$\left.\begin{gathered} l = \epsilon^{-a} l^*, \quad z = \pi/(2\hat{m}) + \epsilon^b z^*, \quad \hat{U} = \epsilon^{-1}\hat{U}^*, \quad \hat{T} = \epsilon^{-2}\hat{T}^*, \quad \hat{S} = \epsilon^{-2}\hat{S}^*, \\ H = \epsilon^{-1}, \quad R_T = \epsilon^{-2} R_T^*, \quad R_S = \epsilon^{-2} R_S^*, \quad \theta = \epsilon\theta^*. \end{gathered}\right\} \tag{4.1}$$

Here the origin in the vertical z-direction has been shifted to the centre of the region of instabilities. Substituting this rescaling into (2.15)–(2.20) leads to the following set of equations for the marginally stable perturbation:

$$\frac{1}{\sigma}[qu' + \epsilon^{-1}\hat{m}u'\hat{U}^*] = \epsilon\theta^*(T' - S') - \epsilon^{-2a} l^{*2} u' + \epsilon^{-2b}\frac{\partial^2 u'}{\partial z^{*2}}, \tag{4.2}$$

$$\frac{1}{\sigma}[qv'] = -\mathrm{i}\epsilon^{-a} l^* p' - \epsilon^{-2a} l^{*2} v' + \epsilon^{-2b}\frac{\partial^2 v'}{\partial z^{*2}}, \tag{4.3}$$

$$\frac{1}{\sigma}[qw'] = -\epsilon^{-b}\frac{\partial p'}{\partial z^*} + (T' - S') - \epsilon^{-2a} l^{*2} w' + \epsilon^{-2b}\frac{\partial^2 w'}{\partial z^{*2}}, \tag{4.4}$$

$$\mathrm{i}\epsilon^{-a} l^* v' + \epsilon^{-b}\frac{\partial w'}{\partial z^*} = 0, \tag{4.5}$$

$$qT' - \epsilon^{-2}\hat{m}w'\hat{T}^* \cos\epsilon^b\hat{m}z^* + \epsilon^{-1}u'(1+\theta^* R_T^*) + w'(\epsilon^{-2}R_T^* - \theta^*) = -\epsilon^{-2a}l^{*2}T' + \epsilon^{-2b}\frac{\partial^2 T'}{\partial z^{*2}}, \tag{4.6}$$

$$qS' - \epsilon^{-2}\hat{m}w'\hat{S}^* \cos\epsilon^b\hat{m}z^* + \epsilon^{-1}u'(1+\theta^* R_S^*) + w'(\epsilon^{-2}R_S^* - \theta^*) = \tau\left(-\epsilon^{-2a}l^{*2}S' + \epsilon^{-2b}\frac{\partial^2 S'}{\partial z^{*2}}\right). \tag{4.7}$$

Here q is the growth rate of the fastest growing intrusions (see Holyer 1983). The relative scales of the perturbations have not yet been established. However it is clear that the terms involving q should not be present at leading order since $q = O(1)$ at marginal stability. From (4.2) we can see that size of u' is at least a factor of ϵ smaller than T' and S', and so the terms involving u' in (4.6) and (4.7) can be neglected. When all these terms are omitted, and the cosine terms expanded as a power series in z^*, the resulting equations at leading order can be written as

$$0 = -\mathrm{i}\epsilon^{-a}l^* p' - \epsilon^{-2a}l^{*2}v' + \epsilon^{-2b}\frac{\partial^2 v'}{\partial z^{*2}}, \tag{4.8}$$

$$0 = -\epsilon^{-b}\frac{\partial p'}{\partial z^*} + (T' - S') - \epsilon^{-2a}l^{*2}w' + \epsilon^{-2b}\frac{\partial^2 w'}{\partial z^{*2}}, \tag{4.9}$$

$$\mathrm{i}\epsilon^{-a}l^* v' + \epsilon^{-b}\frac{\partial w'}{\partial z^*} = 0, \tag{4.10}$$

$$w'(\epsilon^{-2}(R_T^* - \hat{m}\hat{T}^*) - \epsilon^{-2+2b}\hat{m}\hat{T}^*(\epsilon^b\hat{m}z^*)^2/2) = -\epsilon^{-2a}l^{*2}T' + \epsilon^{-2b}\frac{\partial^2 T'}{\partial z^{*2}}, \tag{4.11}$$

$$w'(\epsilon^{-2}(R_S^* - \hat{m}\hat{S}^*) - \epsilon^{-2+2b}\hat{m}\hat{S}^*(\epsilon^b\hat{m}z^*)^2/2) = \tau\left(-\epsilon^{-2a}l^{*2}S' + \epsilon^{-2b}\frac{\partial^2 S'}{\partial z^{*2}}\right). \tag{4.12}$$

Lastly, by dividing (4.12) by τ, subtracting it from (4.11) and defining a new quantity $T^\dagger = T' - S'$, equations (4.9), (4.11) and (4.12) are replaced by the pair of equations

$$0 = -\epsilon^{-b}\frac{\partial p}{\partial z^*} + T^\dagger - \epsilon^{-2a}l^{*2}w' + \epsilon^{-2b}\frac{\partial^2 w'}{\partial z^{*2}}, \tag{4.13}$$

$$w'(\epsilon^{-2}((R_T^* - \hat{m}\hat{T}^*) - (R_S^* - \hat{m}\hat{S}^*)/\tau) - \epsilon^{-2+2b}\hat{m}(\hat{T}^* - \hat{S}^*/\tau)(\hat{m}z^*)^2/2) = -\epsilon^{-2a}l^{*2}T^\dagger + \epsilon^{-2b}\frac{\partial^2 T^\dagger}{\partial z^{*2}}. \tag{4.14}$$

These last two equations, along with (4.8) and (4.10) are essentially equivalent to the equations for penetrative convection with a cubic vertical temperature profile studied by Matthews (1988) when the growth rate is zero. All that is needed now is to find the correct rescalings. One result that we can apply immediately from Matthews is that the magnitude of horizontal and vertical scales of the instabilities is the same, hence $a = b$.

We have yet to determine the behaviour of $\hat{T}^*$ and $\hat{S}^*$ except to say that they are $O(1)$ at leading order. We will pose an expansion

$$\hat{T}^* = \hat{T}_0^* + \epsilon^c\hat{T}_1^* + \cdots, \qquad \hat{S}^* = \hat{S}_0^* + \epsilon^c\hat{S}_1^* + \cdots. \tag{4.15}$$

In order to recover Matthews' equations we must have a balance between the constant and quadratic term multiplying w' in (4.14). This implies that either $a = 0$ or that at

leading order the constant term was zero. If a were zero then (4.13) would imply that w' and $T^\dagger$ were of the same magnitude, but this is clearly not the case in (4.14) and so we must discount this possibility. Hence we must have

$$(R_T^* - \hat{m}\hat{T}^*) - (R_S^* - \hat{m}\hat{S}^*)/\tau$$
$$= (R_T^* - R_S^*/\tau) - \hat{m}(\hat{T}_0^* - \hat{S}_0^*/\tau) - \epsilon^c \hat{m}(\hat{T}_1^* - \hat{S}_1^*/\tau) + \cdots = O(\epsilon^{2a}), \quad (4.16)$$

giving

$$R_T^* - R_S^*/\tau = \hat{m}(\hat{T}_0^* - \hat{S}_0^*/\tau) \quad (4.17)$$

and

$$c = 2a. \quad (4.18)$$

We can now rewrite (4.14) as

$$-w'\epsilon^{-2+2a}(\hat{m}(\hat{T}_1^* - \hat{S}_1^*/\tau) - (R_T^* - R_S^*/\tau)(\hat{m}z^*)^2/2) = -\epsilon^{-2a} l^{*2} T^\dagger + \epsilon^{-2a}\frac{\partial^2 T^\dagger}{\partial z^{*2}}. \quad (4.19)$$

Since we need balances between the terms involving w' and $T^\dagger$ in both (4.19) and (4.13) we see that

$$a = 1/3. \quad (4.20)$$

This tells us that in contrast to the two-dimensional asymptotics of Kerr (1992) the size of the instabilities decreases as the ratio of the horizontal gradients to the vertical gradients decreases.

If we rescale all the variables we can obtain an exact correspondence with the equations of Matthews (1988) restricted to two dimensions, and so we can use his results to give the horizontal wavenumber for the onset of instability. This rescaling gives

$$l = k_c \epsilon^{-1/3}\left(\frac{\hat{m}^2(R_S^*/\tau - R_T^*)}{6R_c}\right)^{1/6}, \quad (4.21)$$

where $k_c = 1.26$ and $R_c = 88.0$ are the critical wavenumber and Rayleigh number found by Matthews. Thus on the logarithmic plot of figure 5 the wavenumber for these disturbances should approach a line of slope $-1/3$ as the Rayleigh number ratio decreases. This is shown by the dashed line, showing good agreement with the numerical results.

The other possibility is that the initial instability is oscillatory. By a similar argument to the above it may be anticipated that such instabilities would grow in regions where the local modified gradients satisfied the conditions for overstable instabilities. In such a case the more complicated analysis of Walton (1982) for the structure of oscillatory instabilities in a fluid with varying vertical salinity gradients would be appropriate. This would be the case when the amplitude of the interleaving satisfied

$$R_T \pm \hat{m}\hat{T} = \frac{\sigma + \tau}{\sigma + 1}(R_S \pm \hat{m}\hat{S}). \quad (4.22)$$

By comparing the amplitude of the intrusions required for this instability to the amplitude for a salt-fingering instability given by (4.17) we find salt-finger convection will occur first if $R_T = 0$. However there are other parameter regimes where the initial instability can indeed be oscillatory.

5. Conclusion

We have looked at the instability of steady double-diffusive intrusions which are parallel to the fastest growing modes. We have found that the fastest growing instabilities nearly always consist of modes which are independent of the horizontal coordinate in the direction perpendicular to the horizontal temperature and salinity gradients driving the intrusions, and which were investigated in Kerr (1992). Only for relatively strong horizontal gradients were instabilities perpendicular to these preferred. In no case was it found that instabilities with other orientations were faster growing. This would seem to give reassurance that many of the experiments where the primary or sole method of visualization consists of looking perpendicularly to these gradients have not missed any important dynamics, and that the two-dimensional numerical simulations are realistic. However, just as with the results of Kerr, the limitations of the current analysis should be borne in mind.

The analysis here looks at the stability of a steady finite-amplitude intrusion that is parallel to the fastest growing mode. This steady mode is clearly not the one that an observer would expect to see. Kerr (1992) observed that the growth rate of the secondary modes of instability significantly exceeds that of the fastest growing mode for amplitudes of the intrusions not much bigger than the marginal modes considered, and so these instabilities are likely to be important even for the fastest growing modes. This holds true for the three-dimensional instabilities examined here. However, the difference between the growth rates of the modes with $l = 0$ and $k = 0$ are never that great, and so it is possible that when it is the fastest growing modes that are present the rôles may be reversed. This small difference in the stability of the $l = 0$ and $k = 0$ modes also backs up Kerr's conclusion that shear is not an important mechanism in the development of the secondary instabilities as the shear terms are absent in the $k = 0$ case.

The other limitation of this analysis when looking at laboratory experiments and numerical simulations is that intrusions are never infinite in length. The layered convection observed is limited in size either by the extent of the apparatus or the time that instabilities take to grow. Thus the two- and three-dimensional secondary instabilities may not be free to select the fastest growing modes of instability. If the container is wider in the direction perpendicular to the horizontal gradients then this may favour the three-dimensional modes of instability. This is certainly true in the experiments of Biello (1997).

An additional effect that may favour the three-dimensional instabilities in experiments is that if the temperature of a wall bounding a stratified fluid is raised quickly, then initially the horizontal gradients of temperature and salinity can be greater that the vertical gradients even if they subsequently become smaller. We have seen that this may favour the initial formation of the three-dimensional modes, which once established may inhibit the growth of the two-dimensional instabilities when the relative size of the horizontal gradients reduces and the two-dimensional disturbances would otherwise be favoured. This is even more likely to be the case near the horizontal boundaries in experiments in rectangular enclosures. Near these boundaries the salinity gradient is usually weaker due to the walls being impermeable to salt.

It is clear from the experiments of Chen & Chen (1997) and Biello (1997) that three-dimensional disturbances do appear in double-diffusive intrusions driven by horizontal temperature and salinity gradients. Unfortunately the ratios of the local Rayleigh numbers associated with the onset of these three-dimensional instabilities in these experiments is not clear. In order to get a better understanding of when they occur in finite enclosures it may be necessary to conduct some fully three-dimensional

numerical simulations, or to perform a stability analysis of steady finite-amplitude convection in a more realistic geometry. The stability of finite-amplitude convection in a rectangular container to two-dimensional disturbances has been addressed by Tsitverblit & Kit (1993), but not to three-dimensional ones. Both of these avenues of research are beyond the scope of this paper.

REFERENCES

Batchelor, G. K. & Nitsche, J. M. 1991 Instability of stationary unbounded stratified fluid. *J. Fluid Mech.* **227**, 357–391.

Biello, J. A. 1997 Aspects of double diffusion in a thin vertical slot. In *Double Diffusive Processes, 1996 Summer Study Programme in Geophysical Fluid Dynamics, Woods Hole Oceanog. Inst. Tech. Rep.* WHOI-97-10.

Chen, C. F., Briggs, D. G. & Wirtz, R. A. 1971 Stability of thermal convection in a salinity gradient due to lateral heating. *Intl J. Heat Mass Transfer* **14**, 57–65.

Chen, C. F. & Chen, F. 1997 Salt-finger convection generated by lateral heating of a solute gradient. *J. Fluid Mech.* **352**, 161–176.

Dijkstra, H. A. & Kranenborg, E. J. 1998 On the evolution of double-diffusive intrusions into a stably stratified liquid: the physics of self-propagation. *Intl J. Heat Mass Transfer* **41**, 2113–2124.

Holyer, J. Y. 1981 On the collective instability of salt fingers. *J. Fluid Mech.* **110**, 195–207.

Holyer, J. Y. 1983 Double-diffusive interleaving due to horizontal gradients. *J. Fluid Mech.* **137**, 347–362.

Holyer, J. Y., Jones, T. J., Priestly, M. G. & Williams, N. C. 1987 The effect of vertical temperature and salinity gradients on double-diffusive interleaving. *Deep-Sea Res.* **34**, 517–530.

Kerr, O. S 1992 Two-dimensional instabilities of steady double-diffusive interleaving. *J. Fluid Mech.* **242**, 99–116.

Kranenborg, E. J. & Dijkstra, H. A. 1998 On the evolution of double-diffusive intrusions into a stably stratified liquid: a study of the layer merging process. *Intl J. Heat Mass Transfer* **41**, 2743–2756.

Matthews, P. C. 1988 A model for the onset of penetrative convection. *J. Fluid Mech.* **188**, 571–583.

Schladow, S. G., Thomas, E. & Koseff, J. R. 1992 The dynamics of intrusions into a thermohaline stratification. *J. Fluid Mech.* **236**, 127–165.

Stern, M. E. 1960 The 'salt fountain' and thermohaline convection. *Tellus* **12**, 172–175.

Stern, M. E. 1967 Lateral mixing of water masses. *Deep-Sea Res.* **14**, 747–753.

Tanny, J. & Tsinober, A. B. 1988 The dynamics and structure of double-diffusive layers in sidewall-heating experiments. *J. Fluid Mech.* **196**, 135–156.

Thorpe, S. A., Hutt, P. K. & Soulsby, R. 1969 The effects of horizontal gradients on thermohaline convection. *J. Fluid Mech.* **38**, 375–400.

Tsinober, A. B., Yahalom, Y. & Shlien, D. J. 1983 A point source of heat in a stable salinity gradient. *J. Fluid Mech.* **135**, 199–217.

Tsitverblit, N. & Kit, E. 1993 The multiplicity of steady flows in confined double-diffusive convection with lateral heating. *Phys. Fluids* A **5**, 1062–1064.

Walton, I. C. 1982 Double-diffusive convection with large variable gradients. *J. Fluid Mech.* **125**, 123–135.